LOGIC (JOURNAL ENGINEERING DESIGN AND TECHNOLOGY)
Journal Engineering Design and Technology
Vol. 26 No.2 July 2026 ; p. 158 - 167
Journal Homepage : http://ojs2.pnb.ac.id/index.php/LOGIC
p-ISSN : 1412-114X e-ISSN : 2580-5649

Numerical Analysis of Outlet Number Effects on Temperature Distribution in a Briquette Oven Using CFD

1) Prodi Teknik Mesin, Fakultas Teknik, Universitas Muhammadiyah Gresik, Gresik, Indonesia
2) D3 Teknik Mesin, Jurusan Teknik Mesin, Politeknik Negeri Malang, Malang, Indonesia
3) Prodi Teknik Mesin, Fakultas Teknik, Universitas Muhammadiyah Gresik, Gresik, Indonesia

Corresponding email [1)*] : alvianihesthi@umg.ac.id

Alviani Hesthi Permata Ningtyas [1)*], Siti Duratun Nasiqiati Rosady [2)], Muhammad Wildanus Sholih [3)]

Abstract. The performance of briquette drying systems is strongly influenced by airflow distribution and thermal uniformity within the drying chamber, which are governed by outlet configuration and internal flow patterns. However, limited studies have systematically quantified the effect of exhaust outlet arrangements on the coupled heat transfer and fluid flow behavior in industrial-scale briquette ovens. This study aims to numerically investigate the influence of single-, double-, and four-outlet configurations on airflow characteristics, temperature distribution, and overall thermal performance of a briquette drying oven. A three-dimensional geometric model representing the combustion chamber, drying chamber, and briquette racks was developed and analyzed using Computational Fluid Dynamics (CFD). Steady-state simulations were performed in ANSYS Fluent employing the standard k–ε turbulence model, with air properties, inlet velocity (9.97 m/s), and thermal boundary conditions defined based on operational data. The results reveal that outlet configuration significantly affects flow recirculation intensity and temperature uniformity across the briquette racks. The four-outlet configuration produced the most homogeneous airflow distribution and reduced thermal gradients, thereby enhancing convective heat transfer effectiveness compared to single- and double-outlet designs. Conversely, the single-outlet case exhibited pronounced recirculation zones and localized temperature variations, potentially leading to uneven drying. These findings demonstrate that optimizing outlet arrangement is a critical design parameter for improving drying efficiency and energy utilization in briquette oven systems, providing a validated numerical framework for future thermal system optimization.

Keywords : Computational Fluid Dynamics, Heat Transfer, Outlet Configuration.

1. INTRODUCTION

The drying process of briquettes represents a critical stage in biomass thermal processing[1]–[3], where moisture removal occurs through coupled heat and mass transfer mechanisms[4]–[7]. Proper drying significantly improves calorific value, mechanical integrity, storage stability, and combustion performance, thereby enhancing the viability of briquettes as a sustainable alternative energy source. Achieving uniform temperature distribution and efficient heat transfer within the drying chamber is essential to prevent uneven drying, cracking, or quality degradation of the final product[8]–[11].

Previous studies have investigated various drying technologies[3], [12]–[20], including solar-assisted and forced-convection systems, highlighting the importance of airflow management in improving drying efficiency. While these studies report improvements in thermal performance and moisture removal rates, limited attention has been given to the influence of exhaust outlet configuration on internal airflow structure and temperature uniformity. In forced-convection drying ovens, outlet placement plays a crucial role in controlling flow recirculation patterns, pressure distribution, and convective heat transfer across product racks. However, systematic numerical investigations comparing different outlet arrangements under identical operating conditions remain scarce.

Furthermore, experimental evaluation of airflow and temperature distribution inside industrial drying chambers is often challenging due to measurement limitations and spatial constraints. Computational Fluid Dynamics (CFD) offers a robust alternative by enabling detailed visualization of velocity fields, thermal gradients, and recirculation zones within complex geometries[1], [3], [4], [19], [20].

Therefore, this study aims to numerically investigate the influence of single-, double-, and four-outlet configurations on airflow characteristics and temperature distribution inside a briquette drying oven. By employing three-dimensional CFD simulations under steady-state forced convection conditions, this research provides a comparative assessment of outlet designs and identifies the configuration that ensures the most uniform thermal environment. The findings contribute to the optimization of drying chamber design and support the development of more efficient biomass drying systems.

Although briquette drying is fundamentally governed by coupled heat and mass transfer processes, the present study focuses exclusively on the thermal-fluid behavior within the drying chamber. The primary objective is to investigate how different outlet configurations influence airflow distribution, temperature uniformity, and convective heat transfer characteristics. Moisture transport, evaporation mechanisms, and drying kinetics were not included in the present numerical model and are therefore beyond the scope of this investigation. Nevertheless, improving temperature uniformity is expected to provide favorable thermal conditions for subsequent moisture removal. Future work will incorporate coupled heat-and-mass transfer modeling to predict moisture distribution and drying kinetics more comprehensively.

2. METHODS

2.1 Geometrical Modeling and Configurations

A three-dimensional model of the briquette drying oven was developed using Autodesk Inventor 2025 based on actual industrial dimensions. The system consists of a combustion chamber, a drying chamber, insulated steel walls, and multiple briquette holding racks. The oven has a total internal area of 6 m², as summarized in Table 1. To evaluate the effect of exhaust design,

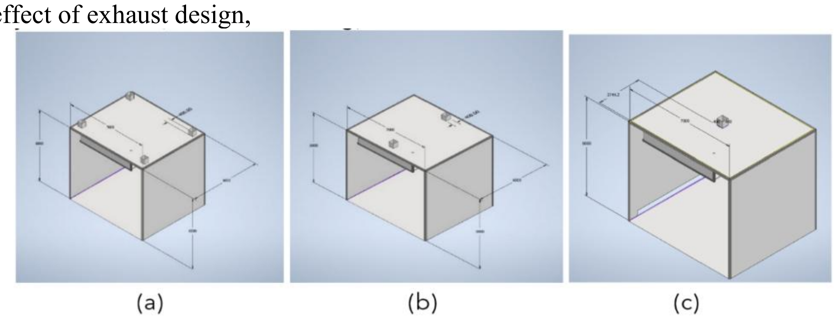

Figure 1. Temperature distribution on the YZ plane for: (a) single outlet, (b) double outlet and (c) four outlets

As illustrated in Figure 1(a–c), the outlet positions were varied on the top surface while maintaining identical chamber geometry and inlet conditions. This approach ensured that performance differences were solely attributed to outlet arrangement. The CAD models were exported in STEP format and imported into ANSYS Workbench for Computational Fluid Dynamics (CFD) analysis.

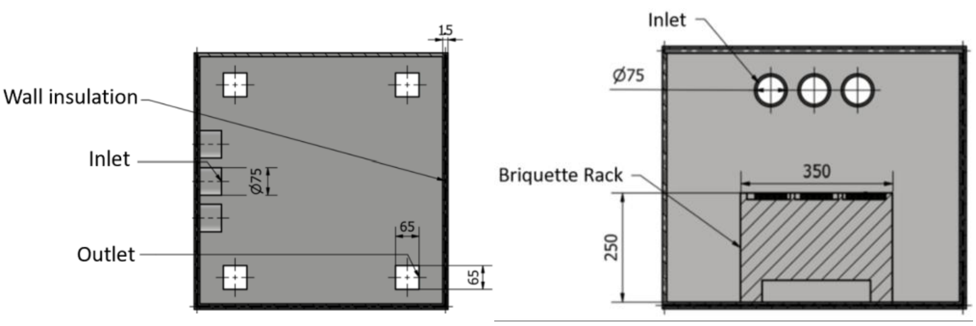

Figure 2. (a)Top View and (b) front view on four outlet oven

The technical drawing in Figure 2 provides the orthogonal views of a four-outlet industrial oven, detailing its top and front configurations alongside a 15 mm thick thermal wall insulation layer. The flow system consists of three parallel inlets with a diameter Ø75 mm on the left wall that feed into the heating chamber from combustion chamber, which then exhaust symmetrically via four 65 mm × 65 mm square outlets situated at the corners. Furthermore, the front view reveals that a 350 mm wide briquette rack is positioned at a height of 250 mm within the oven cavity, directly beneath the horizontally aligned inlet ports to intercept the incoming convective airflow.

Table 1. Geometry Spesification

Descriptions	Value
Oven length	7000 mm
Width	3000 mm
Height	6000 mm
Wall Material	Coated Stell
Inlet diameter	75 cm
Outlet size	65 x 65 cm
Insulation	Glasswool thk. 1.5 mm
Rack dimension	90 x 250 x 350 cm
Capacity	5 Tons

The data provided in Tabel 1. shows the structural and geometric specifications of an industrial oven with an overall capacity of 5 Tons. Constructed with coated steel walls, the primary dimensions of the oven cavity span a length of 7000 mm, a width of 3000 mm, and a height of 6000 mm, supplemented by a 1.5 mm thick glasswool insulation layer. The thermal processing chamber also features a 75 cm inlet diameter, 65 x 65 cm outlets, and houses an internal rack with dimensions of 90 x 250 x 350 cm.

2.2. Governing Equations and Physical Modeling

The airflow and heat transfer inside the drying chamber were modeled using the steady-state, three-dimensional Reynolds-Averaged Navier–Stokes (RANS) equations for incompressible flow[21]–[25]. The governing continuity equation is expressed as Eq. (1)

$$\nabla \cdot u = 0 \tag{1}$$

ensuring mass conservation. The momentum equations are written as Eq. (2)

$$\rho(u \cdot \nabla)u = -\nabla p + \nabla \cdot [(\mu + \mu_t)(\nabla u + \nabla u^T)] + \rho g \tag{2}$$

where ρ is the fluid density, u is the velocity vector, p is the pressure, μ is the dynamic viscosity, and μ_t is the turbulent (eddy) viscosity. Heat transfer is governed by the energy equation as Eq. (3)

$$\rho c_p(\mathbf{u} \cdot \nabla)T = \nabla \cdot \left[\left(k + \frac{\mu_t c_p}{Pr_t}\right)\nabla T\right] + S_T \tag{3}$$

where T is temperature, c_p the specific heat capacity, k is the thermal conductivity, and Pr_t is the turbulent Prandtl number[26], [27]. Turbulence effects were represented using the standard k_ε model, in which the turbulent viscosity is defined as Eq. (4)

$$\mu_t = \rho C_\mu \frac{k^2}{\varepsilon} \tag{4}$$

The transport equations for turbulent kinetic energy (k) and its dissipation rate (ε) are solved to close the RANS system, incorporating production and dissipation terms with the standard model constants $C_\mu = 0.09$, $C_{1\varepsilon} = 1.44$, $C_{2\varepsilon} = 1.92$, $\sigma_k = 1.0$, and $\sigma_\varepsilon = 1.3$. This formulation ensures reliable prediction of internal forced convection and thermal distribution within the drying chamber[28]–[32].
Air was defined as a Newtonian fluid with properties listed in Table 2.

Table 2. Data input for reference value

Descriptions	Value
Area of Oven (A)	6 m^2
Dynamic Viscosity (μ)	1.7894×10^{-5} kg/(m·s)
Temperature (T)	40,3 °C
Velocity (v)	9,97 m/s
Density (ρ)	1,225 Kg/m^3

The total heat transfer rate was evaluated using the surface integral function available in ANSYS Fluent. The calculation was performed by integrating the local wall heat flux over all heated internal surfaces of the drying chamber according to Eq. 5 below

$$Q = \int_A q'' \; dA \quad (5)$$

where Q is the total heat transfer rate (W), q" is the local wall heat flux (W/m²), and A represents the heated wall surface area.

The total heat transfer rate was extracted using the Reports then Surface Integrals then Total Heat Transfer Rate function in ANSYS Fluent after the numerical solution had reached convergence. The evaluated surfaces included the heated chamber walls and the combustion-side heat transfer surfaces that supplied thermal energy to the drying chamber. The reported values therefore represent the net convective heat transferred from the heated walls to the circulating air under steady-state operating conditions.
Since the numerical simulations were conducted under steady-state conditions, the reported heat transfer rate corresponds to the converged solution rather than a transient time-dependent response.

2.3. Mesh Generation
The computational domain, shown schematically in Figure 2, includes the blower inlet, drying racks, and outlet ducts.

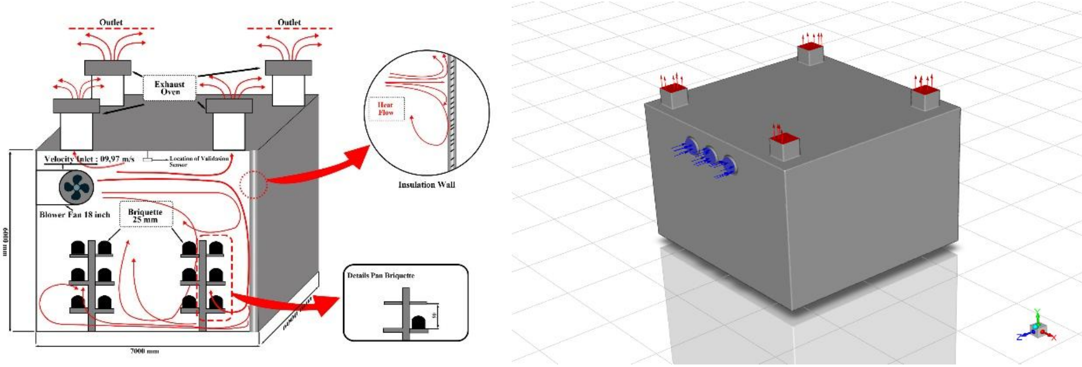

(a) (b)

Figure 3. (a) Schematic and (b) CFD Model of the Forced-Convection Briquette Drying Chamber

The figure 3 illustrates the geometric configuration and airflow characteristics of a forced-convection briquette drying chamber used for thermal performance evaluation. Figure 3.(a) presents the internal arrangement, including an 18-inch blower fan generating an inlet air velocity of approximately 10 m/s, vertically stacked briquettes, exhaust outlets positioned at the top surface, and insulated chamber walls to minimize heat loss. The airflow pattern indicates recirculation zones near the lower region and along the side walls, suggesting potential non-uniform temperature and velocity distributions within the drying space. The three-dimensional CFD model (right) represents the computational domain with defined inlet and outlet boundary conditions, enabling detailed simulation of internal flow structures and heat transfer mechanisms. Collectively, the model highlights the influence of chamber geometry, insulation, and forced airflow on convective heat transfer effectiveness and drying uniformity.

Table 3. Grid Indepedence

Geometry	Cells (million)	Skewness Mesh	THTR [W]	Temperature Thermocouple °C	Error %
Oven 4 Outlet Mesh 1	1.4	0.79889	932	78.5	0.64
Oven 4 Outlet Mesh 2	1.5	0.81121	909	82	-3.66
Oven 4 Outlet Mesh 3	2.1	0.79999	863	79.1	-0.13
Oven 4 Outlet Mesh 4	2.5	0.82122	911	83	-4.82

The data in Table 3. Grid Independence presents a mesh independence study evaluating four different computational grids (Mesh 1 to Mesh 4) for the four-outlet oven geometry based on cell count, skewness, total heat transfer rate (THTR), thermocouple temperature, and percentage error. Mesh 1 consists of 1.4 million cells with a mesh skewness of 0.79889, yielding a total heat transfer rate of 932 W and a thermocouple temperature of 78.5°C, which results in a low relative error of 0.64%. Despite having the coarsest resolution among the tested configurations, Mesh 1 represents a highly favorable choice for the final simulation because it balances numerical accuracy with computational efficiency, providing reliable thermal prediction metrics while keeping computational resource demands to a minimum.

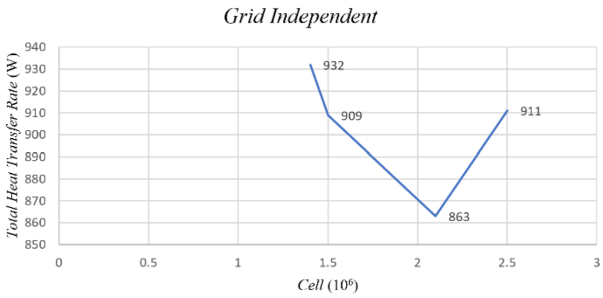

Figure 4. Grid Independence Index

The figure 4 presents the grid independence analysis showing the variation of total heat transfer rate with increasing mesh cell numbers. As the mesh is refined beyond approximately 2.1 × 10^6 cells, the predicted heat transfer rate stabilizes with minimal deviation, indicating that the solution has reached grid-independent behavior.

Special attention was given to boundary layer resolution to capture velocity and thermal gradients.

(a) (b)

Figure 5. Experimental Briquette Drying Oven Used for CFD Validation (a) oven front view and (b) blower

The figure 5. presents the actual forced-convection briquette drying oven employed for experimental validation of the CFD simulation results. Figure 5. (a) shows the internal drying chamber equipped with multi-level trays for briquette placement, allowing evaluation of temperature and airflow distribution across different vertical positions. Figure 5(b) illustrates the axial blower fan installed to generate forced air circulation within the chamber. This experimental setup was used to measure airflow temperature profiles, providing validation data for comparison with numerical predictions and ensuring the reliability and accuracy of the thermal-fluid simulation model.

3. RESULTS AND DISCUSSION

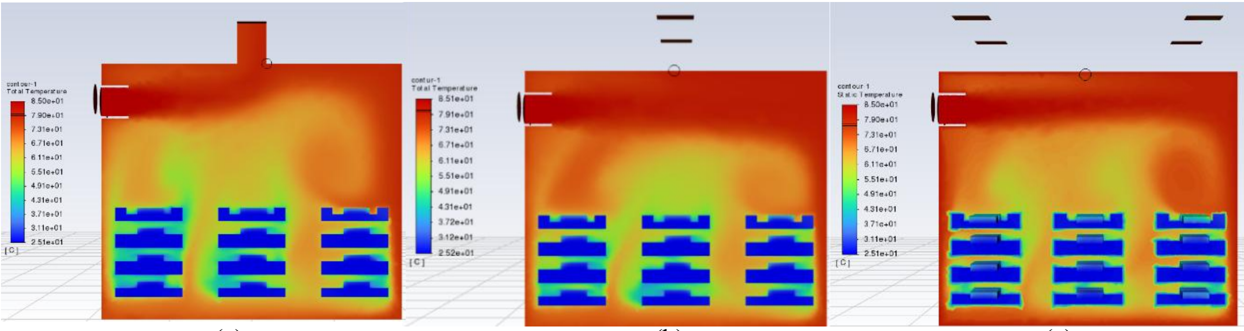

(a) (b) (c)

Figure 6. Temperature distribution YZ plane on (a) 1 outlet, (b) 2 outlets and (c) 4 outlets.

Figure 6 compares the static temperature distribution inside the drying chamber for three exhaust configurations: (a) single exhaust, (b) dual exhausts, and (c) four exhausts. In the single-exhaust configuration as figure 6.(a) pronounced thermal gradient is observed, with significant temperature accumulation in the upper region and non-uniform heat penetration toward the briquette layers. This indicates limited air circulation and localized heat stagnation. When two exhausts are applied as figure 6.(b), the temperature field becomes more evenly distributed, although moderate stratification remains near the central upper zone, suggesting partial improvement in convective heat removal. In contrast, the four-exhaust configuration as figure 6.(c) demonstrates the most uniform temperature distribution, characterized by reduced hot spots near the ceiling and more homogeneous heat diffusion around the briquette stacks. The enhanced uniformity indicates improved airflow circulation and more effective convective heat transfer, leading to better thermal balance within the chamber. Overall, increasing the number of exhaust outlets significantly mitigates thermal stratification and promotes more consistent drying conditions.

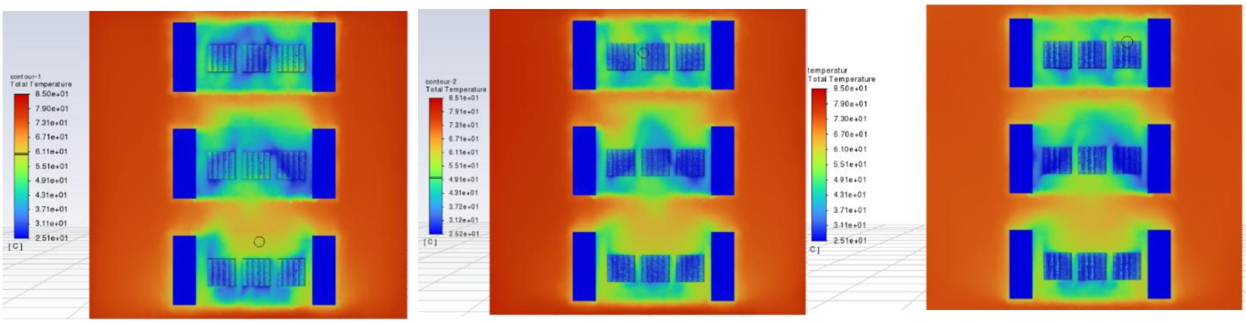

(a) (b) (c)

Figure 7. Temperature distribution plane XZ on (a) 1 outlet, (b) 2 outlets and (c) 4 outlets.

Figure 7 presents the temperature distribution on the XZ plane for configurations with (a) 1 exhaust, (b) 2 exhausts, and (c) 4 exhausts inside the drying chamber. In the single-exhaust configuration, the heat distribution appears less uniform, with high-temperature regions concentrated in specific areas, whereas increasing the number of exhausts to two and four improves temperature uniformity around the drying racks. The four-exhaust configuration demonstrates the most homogeneous thermal distribution and reduces extreme temperature gradients, indicating its potential to enhance drying uniformity and overall thermal performance.

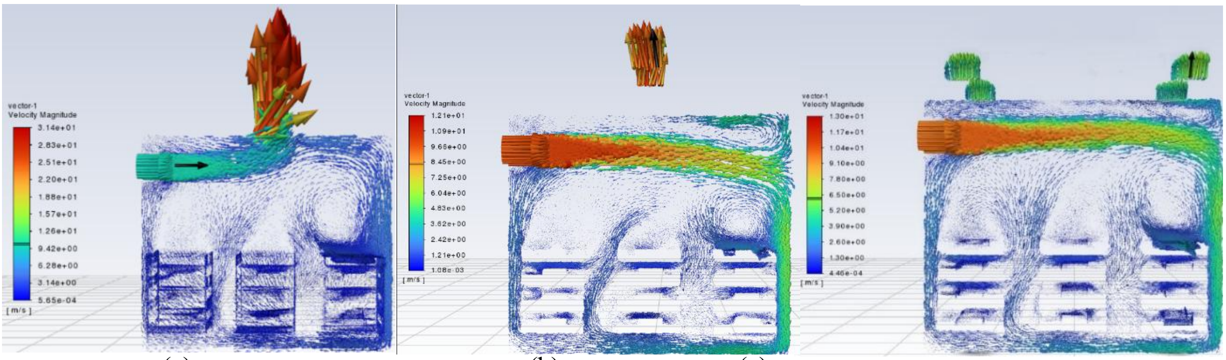

(a) (b) (c)

Figure 8. Velocity vector on ZX plane in (a) 1 outlet, (b) 2 outlets and (c) 4 outlets.

Figure 8 shows that the highest velocity regions are concentrated near the inlet duct and exhaust outlets, indicated by the red–orange vectors, where the airflow is directly driven by the blower and extracted through the vents. In contrast, low-velocity zones (blue regions) are observed inside the chamber, particularly around the lower racks and corner areas, where recirculation and flow stagnation occur. As the number of exhausts increases from one to four, the high-velocity jet becomes more distributed along the upper section, while low-velocity regions inside the chamber are reduced, resulting in more uniform airflow circulation.

To complement the qualitative interpretation of the temperature contours, the thermal performance of each outlet configuration was quantitatively evaluated using four representative parameters: maximum temperature, minimum temperature, average temperature, and total heat transfer rate. These parameters provide an objective assessment of the influence of outlet arrangement on heat distribution and convective heat transfer inside the briquette drying chamber.

Tabel 4. Quantitative thermal performance comparison for different outlet configurations.

Parameter	1 Outlet	2 Outlets	4 Outlets
Maximum Temperature (°C)	79.0	79.1	77.0
Minimum Temperature (°C)	35.0	37.0	57.0
Average Temperature (°C)	39.0	41.0	42.0
Total Heat Transfer Rate (W)	3322	4720	4754

The quantitative results presented in Table 4 demonstrate that the outlet configuration significantly influences the thermal performance of the drying chamber. The maximum temperature remains relatively constant, ranging from 77.0°C to 79.1°C, indicating that the heat source supplies nearly the same thermal energy in all configurations. Therefore, the primary effect of increasing the number of outlets is not to increase the peak temperature, but rather to improve the distribution of heat within the drying chamber.

A more pronounced difference is observed in the minimum temperature. The minimum temperature increases from 35.0°C in the single-outlet configuration to 37.0°C in the double-outlet configuration and reaches 57.0°C in the four-outlet configuration. Compared with the single-outlet design, the four-outlet configuration increases the minimum temperature by approximately 62.9%, indicating that cold regions are substantially reduced. This result suggests a significant improvement in temperature uniformity throughout the chamber, which is beneficial for achieving more consistent drying conditions.

The average chamber temperature also increases from 39.0°C for the single outlet to 41.0°C and 42.0°C for the double- and four-outlet configurations, respectively. Although the increase in average temperature is relatively modest, it indicates that thermal energy is distributed more effectively throughout the drying chamber. The higher average temperature, together with the increased minimum temperature, demonstrates that the additional outlets improve thermal utilization without substantially increasing the peak temperature.

The influence of outlet configuration is further confirmed by the total heat transfer rate. The single-outlet configuration produces a total heat transfer rate of 3322 W, whereas the double- and four-outlet configurations achieve 4720 W and 4754 W, respectively. Relative to the single-outlet configuration, the total heat transfer rate increases by approximately 42.1% for the double-outlet configuration and 43.1% for the four-outlet configuration. Although the difference between the double- and four-outlet configurations is relatively small (approximately 0.7%), the four-outlet configuration consistently exhibits the highest heat transfer rate while simultaneously providing the highest minimum temperature and the most uniform thermal field. These results indicate that increasing the number of outlets improves convective heat transfer efficiency and promotes a more homogeneous thermal environment inside the drying chamber.

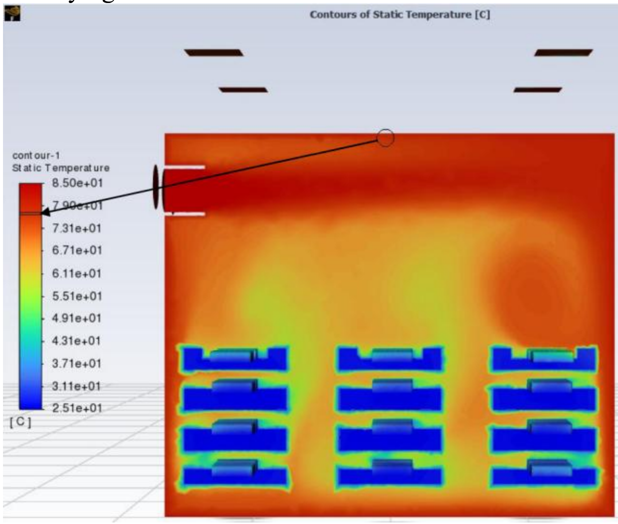

Figure 9. location that take temperature to compare with actual condition

Figure 9 illustrates the static temperature contour on the YZ mid-plane of the oven chamber equipped with four exhaust outlets. This sectional visualization provides insight into the internal thermal field and reveals the spatial temperature gradient along the vertical (Y) and transverse (Z) directions. The distribution demonstrates a relatively uniform thermal region in the core zone, with mild gradients observed near the exhaust boundaries, indicating the influence of convective heat removal on local temperature stratification.

The CFD simulation predicts a representative mid-plane temperature of 78.5°C, whereas experimental measurements obtained under identical operating conditions indicate a temperature of 79°C. The relative deviation between numerical and experimental results was quantified using:

$$\text{Error } (\%) = \frac{T_{\text{oven}} - T_{\text{simulation}}}{T_{\text{simulation}}} \times 100$$

Substitution of the measured values yields:

$$\text{Error } (\%) = \frac{79 - 78.5}{78.5} \times 100 = 0.63\%$$

A discrepancy of only 0.63% confirms a high level of agreement between simulation and experimental data. In heat transfer validation studies, an error below 5% is generally considered acceptable for engineering applications; therefore, the present deviation indicates excellent predictive accuracy of the numerical model.

The minor difference can be attributed to unavoidable experimental uncertainties (thermocouple accuracy and positioning sensitivity), assumptions of uniform material properties, idealized boundary conditions, and potential simplifications in turbulence modeling. Nevertheless, the close correlation suggests that the governing equations for coupled momentum and energy transport were properly resolved and that the mesh and numerical schemes were sufficiently refined to capture the dominant convective heat transfer mechanisms within the drying chamber.

Furthermore, the observed temperature uniformity in the mid-plane implies that the four-exhaust configuration effectively enhances air circulation and reduces localized thermal accumulation. This finding supports the suitability of the current exhaust design for achieving homogeneous drying conditions, which is critical for maintaining briquette quality and minimizing moisture gradients.

Overall, the strong agreement between numerical prediction and experimental measurement validates the robustness of the CFD model and establishes a reliable foundation for subsequent parametric optimization studies involving exhaust arrangement, airflow rate, and thermal efficiency enhancement.

4. CONCLUSION

This study systematically evaluated the influence of exhaust outlet configuration on airflow behavior and thermal performance in a forced-convection briquette drying oven using three-dimensional Computational Fluid Dynamics (CFD) simulations supported by experimental validation. A grid independence study ensured numerical stability, and comparison with measured mid-plane temperatures yielded a relative deviation of only 0.63%, confirming high predictive accuracy of the model. The results demonstrate that outlet configuration significantly affects internal flow topology and temperature uniformity. The single-exhaust design produced strong thermal stratification and localized recirculation zones, leading to uneven heat distribution across briquette layers. The dual-exhaust configuration improved airflow symmetry but still exhibited moderate temperature accumulation near the upper chamber. In contrast, the four-exhaust configuration achieved the most uniform thermal field, minimized stagnant regions, and enhanced convective heat transfer stability during both transient and steady regimes. These findings indicate that exhaust arrangement is a critical design parameter that directly governs convective circulation and drying uniformity rather than serving merely as a structural feature. The validated numerical framework developed in this study provides a practical basis for optimizing industrial biomass drying chambers to improve thermal efficiency and product quality, with future work should incorporate coupled heat-and-mass transfer, moisture diffusion, and drying kinetics to provide a more comprehensive prediction of briquette drying performance. Integrating moisture transport with CFD simulations would enable direct evaluation of drying rate, moisture distribution, and overall thermal efficiency, thereby extending the applicability of the present numerical framework to practical industrial drying processes.

5. ACKNOWLEDGEMENT

The authors would like to express their sincere gratitude to all parties who have supported the completion of this research. The authors gratefully acknowledge the financial support provided by the Directorate of Research and Community Service (DPPM), Universitas Muhammadiyah Gresik.

6. REFERENCES

[1] B. Rayianom, “ANALISIS PERPINDAHAN PANAS PADA OVEN PENGERING BREM GUNA MENINGKATKAN KINERJA DAN EFEKTIVITAS ALAT DENGAN METODE PANAS PADA OVEN PENGERING BREM,” pp. 1–8, 2023.

[2] O. V. No, M. F. Nurrohman, and G. A. Pohan, “Jurnal Mesin Material Manufaktur dan Energi Desain Dan Simulasi Distribusi Panas Pada Oven Untuk Proses Powder coating Menggunakan Ansys Fluent,” vol. 5, no. 2, pp. 75–84, 2025.

[3] G. Bahari, I. S. Irawati, I. A. Hendaryanto, I. Ayu, and P. Pratiwi, “Simulasi Computational Fluid Dynamics (CFD) untuk Optimalisasi Proses Perekatan pada Oven Bambu Laminasi,” vol. 16, no. 01, pp. 232–239, 2025, doi: 10.35970/infotekmesin.v16i1.2567.

[4] I. R. A. Jurnal, T. Mesin, S. M. Rohman, A. Mukhtar, and A. Burhanudin, “Simulasi Laju Aliran Udara pada Mesin Oven Pengering Kerupuk dengan Burner Sederhana Berbasis Computational Fluid Dynamics Simulation of Air Flow Rate in a Cracker Drying Oven Machine with a Simple Burner Based on Computational Fluid Dynamics,” vol. 3, no. 2, pp. 38–47, 2024.

[5] I. R. A. Jurnal, T. Mesin, and J. D. Hasibuan, “Pemodelan Numerik Perpindahan Panas pada Dinding Ruang Bakar Boiler Menggunakan Software Engineering Numerical Modeling of Heat Transfer in Boiler Combustion Chamber Walls Using Software Engineering,” vol. 2, no. 2, pp. 81–90, 2023.

[6] K. M. R. Khadafi, F. Putri, and O. M. Utami, “ANALISIS KEGAGALAN PIPA EMBEDDED PADA PLTU TE 3X10 MW,” vol. 5, no. 2, pp. 48–55, 2024.

[7] N. Titahelu, S. J. Litiloly, J. T. Mesin, F. Teknik, U. Pattimura, and K. Poka-ambon, “Analisis laju kondensasi akibat pengaruh kecepatan udara terhadap karakteristik perpindahan panas pada oven pengering pati sagu kapasitas,” no. April, pp. 108–114, 2018.

[8] R. Sary, “Kaji eksperimental pengeringan biji kopi dengan menggunakan sistem konveksi paksa,” vol. 14, no. 7, pp. 13–18, 2016.

[9] P. P. Menyeluruh, P. Tekanan, M. Iskandar, A. Hakim, and M. Bakrie, “Pengaruh Baffle Cut Pada Shell dan Tube Heat Exchanger Terhadap Koefisien Pengaruh Baffle Cut Pada Shell dan Tube Heat Exchanger Terhadap Koefisien Perpindahan Panas Menyeluruh & Penurunan Tekanan,” no. September, 2024, doi: 10.31851/redoks.v9i2.9089.

[10] F. T. Industri, “ANALISIS PERPINDAHAN PANAS PADA OVEN ELECTRIC HEATERS OVEN FOR DRYING”.

[11] D. Version, “Modelling of Heat Transfer and Fluid Flow in the Hot Section of Gas Turbines Used in Power Generation : A Comprehensive Survey,” 2018, doi: 10.1002/er.4296.

[12] T. R. Steiner, “Results in Engineering High temperature steady-state experiment for computational radiative heat transfer validation using COMSOL and ANSYS,” *Results Eng.*, vol. 13, no. January, p. 100354, 2022, doi: 10.1016/j.rineng.2022.100354.

[13] G. Michael and R. Hulu, “ANALISIS PERPINDAHAN PANAS DAN EFEKTIVITAS ECONOMIZER PADA BOILER UNIT 4 PLTU PANGKALAN SUSU,” vol. 2, no. 1, 2021.

[14] Jeffry, I. Isranuri, M. Sabri, S. Abda, and M. Marragi, “ANALISA SIMULASI DISTRIBUSI TEMPERATUR DAN TEKANAN MENGGUNAKAN APLIKASI ANSYS 15.0 PADA RUANG

BAKAR TURBIN GAS UNTUK MENGETAHUI TINGKAT KEADAAN," no. 3, pp. 67–80, 2019.
[15] A. L. I. Alsharea, E. J. Lavasani, I. Stamatin, C. Diac, and A. Balan, "DESIGNING GEOMETRIES IN SOLIDWORKS FOR HEAT TRANSFER SIMULATIONS IN ANSYS," vol. 902, pp. 1–16, 2025.
[16] S. Perpindahan, P. Pada, D. Ruang, and J. D. Hasibuan, "BAKAR BOILER DENGAN SOFTWARE ANSYS SKRIPSI Oleh : FAKULTAS TEKNIK UNIVERSITAS MEDAN AREA MEDAN SKRIPSI Diajukan sebagai Salah Satu Syarat untuk Memperoleh Gelar Sarjana di Program Studi Teknik Mesin Fakultas Teknik Universitas Medan Area Oleh : JOEL DAVIDSON HASIBUAN FAKULTAS TEKNIK MEDAN," 2023.
[17] JMPQ Delgado, "eat transfer and fluid flo in separation and transport procesesses," Trans Tech Publication, p. 32.
[18] A. R. Wardana, A. Mukhtar, and A. Burhanuddin, "Analisis Persebaran Panas Pada Mesin Oven Pengering Kerupuk Dengan Burner Sederhana Berbasis Computational Fluid Dynamics," vol. 4, no. 2, pp. 15–24, 2024.
[19] Sabiqunassabiqun, "2D ANALYSIS OF THE EFFECT OF OUTLET POSITION IN A DRYING," vol. 2, no. 2, pp. 193–202, 2025.
[20] Z. Khatir *et al.*, "Computational fluid dynamics (CFD) investigation of air flow and temperature distribution in a small scale bread-baking oven," *Appl. Energy*, vol. 89, no. 1, pp. 89–96, 2012, doi: 10.1016/j.apenergy.2011.02.002.
[21] A. Kumar, A. Dewangan, O. Khan, P. Kumar, and N. Kumar, "Influence of ceiling fan induced mass flow rate to create uniform temperature distribution in a closed room : A CFD investigation," *Int. J. Thermofluids*, vol. 26, no. February 2025, p. 101140, 2027, doi: 10.1016/j.ijft.2025.101140.
[22] A. Kumar, A. Dewangan, and O. Khan, "Corrigendum to ' Influence of ceiling fan induced mass flow rate to create uniform temperature distribution in a closed room : A CFD investigation ,'" *Int. J. Thermofluids*, vol. 27, no. March 2025, p. 101156, 2027, doi: 10.1016/j.ijft.2025.101156.
[23] M. Abaee, S. Sohrabi, and M. K. Moraveji, "CFD assisted engineering of spiral microfluidic reactors for room temperature synthesis of ZnO nanoparticles," *Ceram. Int.*, vol. 50, no. 18PA, pp. 32613–32623, 2024, doi: 10.1016/j.ceramint.2024.05.495.
[24] A. Azma and Y. Liu, "Case Studies in Thermal Engineering Enhancing CFD computational efficiency using hybrid data-driven and physics-based modeling," *Case Stud. Therm. Eng.*, vol. 78, no. December 2025, p. 107641, 2026, doi: 10.1016/j.csite.2026.107641.
[25] S. Marashian, O. Abouali, A. Vadiee, and S. Sadrizadeh, "Evaluating the effectiveness of personalized exhaust in minimizing cross contamination in two-bed patient rooms using CFD," *J. Build. Eng.*, vol. 120, no. August 2025, p. 115577, 2026, doi: 10.1016/j.jobe.2026.115577.
[26] S. Tang, J. Zhong, M. Li, Y. Jiang, Y. Zhang, and J. Deng, "Field synergy enhancement of fluid flow and heat transfer in intensive tobacco roasting room," *Comput. Electron. Agric.*, vol. 238, no. August, p. 110837, 2025, doi: 10.1016/j.compag.2025.110837.
[27] X. Chen, Z. Wu, R. Ma, Z. Wang, Z. Wang, and X. Wang, "Wind and thermal comfort performance of the fourth-generation apartment housing in Northern and Southern China based on the 'CFD–APMV' method," *Sustain. Cities Soc.*, p. 107655, 2026, doi: 10.1016/j.scs.2026.107655.
[28] G. Baldinelli, J. Schnotale, F. Bianchi, and A. Lechowska, "Energy & Buildings A variable thermal transmittance adaptive wall : comparison between CFD simulations and experimental tests," *Energy Build.*, vol. 350, no. September 2025, p. 116629, 2026, doi: 10.1016/j.enbuild.2025.116629.
[29] H. Zhao, X. Jian, B. Zhou, W. Li, and Z. Xu, "Energy & Buildings Thermal comfort of medical staff in operating rooms : a review and future perspectives," *Energy Build.*, vol. 364, no. 30, p. 117640, 2026, doi: 10.1016/j.enbuild.2026.117640.
[30] P. Kamma, K. Loksupapaiboon, J. Phromjan, and A. Boekfah, "Optimization of cooking vessel geometry for enhanced flame impingement heat transfer using a hybrid CFD and artificial intelligence approach," *Int. Commun. Heat Mass Transf.*, vol. 178, no. P4, p. 111831, 2026, doi: 10.1016/j.icheatmasstransfer.2026.111831.
[31] H. Wang, K. Qiu, Z. Gao, J. Hang, and J. Shen, "Urban Climate A CFD simulation study on the effect of air-conditioning outdoor units on the wind-thermal environment in street canyons," *Urban Clim.*, vol. 67, no. March, p. 102875, 2026, doi: 10.1016/j.uclim.2026.102875.
[32] A. Ravikumar *et al.*, "An improved CFD wall heat transfer model based on a critical analysis in heavy-duty diesel engines ☆," *Appl. Therm. Eng.*, vol. 302, no. P3, p. 131878, 2026, doi: 10.1016/j.applthermaleng.2026.131878.